Available online at www.sciencedirect.com

SciVerse ScienceDirect

Geochimica et Cosmochimica Acta 96 (2012) 215–229

Geochimica et Cosmochimica Acta

www.elsevier.com/locate/gca

Revised calibration of the MBT–CBT paleotemperature proxy based on branched tetraether membrane lipids in surface soils

Francien Peterse [a,*], Jaap van der Meer [a], Stefan Schouten [a,b], Johan W.H. Weijers [b], Noah Fierer [c,d], Robert B. Jackson [e], Jung-Hyun Kim [a], Jaap S. Sinninghe Damsté [a,b]

[a] *Departments of Marine Organic Biogeochemistry and Marine Ecology, NIOZ Royal Netherlands Institute for Sea Research, PO Box 59, 1790 AB Den Burg, Texel, The Netherlands*

[b] *Department of Earth Sciences, Utrecht University, PO Box 80.021, 3508 TA Utrecht, The Netherlands*

[c] *Department of Ecology and Evolutionary Biology, University of Colorado, Boulder, CO 80309, USA*

[d] *Cooperative Institute for Research in Environmental Sciences, University of Colorado, Boulder, CO 80309, USA*

[e] *Department of Biology, Duke University, Durham, NC 27708-0338, USA*

Received 15 July 2011; accepted in revised form 7 August 2012; available online 23 August 2012

Abstract

The MBT–CBT proxy for the reconstruction of paleotemperatures and past soil pH is based on the distribution of branched glycerol dialkyl glycerol tetraether (brGDGT) membrane lipids. The Methylation of Branched Tetraether (MBT) and the Cyclisation of Branched Tetraether (CBT) indices were developed to quantify these distributions, and significant empirical relations between these indices and annual mean air temperature (MAT) and/or soil pH were found in a large data set of soils. In this study, we extended this soil dataset to 278 globally distributed surface soils. Of these soils, 26% contains all nine brGDGTs, while in 63% of the soils the seven most common brGDGTs were detected, and the latter were selected for calibration purposes. This resulted in new transfer functions for the reconstruction of pH based on the CBT index: $pH = 7.90–1.97 \times CBT$ ($r^2 = 0.70$; RMSE = 0.8; $n = 176$), as well as for MAT based on the CBT index and methylation index based on the seven most abundant GDGTs (defined as MBT′): $MAT = 0.81–5.67 \times CBT + 31.0 \times MBT'$ ($r^2 = 0.59$; RMSE = 5.0 °C; $n = 176$). The new transfer function for MAT has a substantially lower correlation coefficient than the original equation ($r^2 = 0.77$). To investigate possible improvement of the correlation, we used our extended global surface soil dataset to statistically derive the indices that best describe the relations of brGDGT composition with MAT and soil pH. These new indices, however, resulted in only a relatively minor increase in correlation coefficients, while they cannot be explained straightforwardly by physiological mechanisms. The large scatter in the calibration cannot be fully explained by local factors or by seasonality, but MAT for soils from arid regions are generally substantially (up to 20 °C) underestimated, suggesting that absolute brGDGT-based temperature records for these areas should be interpreted with caution.

The applicability of the new MBT′–CBT calibration function was tested using previously published MBT–CBT-derived paleotemperature records covering the last deglaciation in Central Africa and East Asia, the Eocene–Oligocene boundary and the Paleocene–Eocene thermal maximum. The results show that trends remain similar in all records, but that absolute temperature estimates and the amplitude of temperature changes are lower for most records, and generally in better agreement with independent proxy data.

* Corresponding author. Current address: ETH Zürich, Geological Institute, Sonneggstrasse 5, 8092 Zürich, Switzerland. Tel.: +41 44 632 3358.

E-mail address: francien.peterse@erdw.ethz.ch (F. Peterse).

0016-7037/$ - see front matter © 2012 Elsevier Ltd. All rights reserved.
http://dx.doi.org/10.1016/j.gca.2012.08.011

1. INTRODUCTION

The reconstruction of paleotemperatures provides a valuable contribution to our understanding of the climatic changes in the past. The number of proxies that can estimate past continental air temperatures is, however, relatively limited. A large part of the continental temperature records is retrieved from lake sediments, where climate indicators like pollen, chironomids, or diatoms may be preserved (e.g. Colinvaux et al., 1996; Lotter et al., 1997; Kurek et al., 2009). However, many of the available proxies are also sensitive to changes in other environmental parameters besides temperature, which can obscure the temperature signal. Furthermore, not all lakes have archived paleoclimatic changes in their sediments, leaving large areas of land without paleotemperature records.

The distribution of a particular suite of molecules globally occurring in soils, i.e. branched glycerol dialkyl glycerol tetraethers (brGDGTs; Fig. 1), may be useful as a tool to obtain high resolution continental temperature reconstructions (Weijers et al., 2007a). These brGDGTs vary in the amount of methyl branches (4–6) and can contain up to two cyclopentane moieties (Sinninghe Damsté et al., 2000; Weijers et al., 2006). The stereochemistry of their glycerol moieties indicates that they have a bacterial origin (Weijers et al., 2006). The exact type of bacteria that synthesize brGDGTs is not completely understood, but brGDGT-Ia (Fig. 1) was recently identified in two species of *Acidobacteria* (Sinninghe Damsté et al., 2011).

An empirical study of 134 soils from over 90 locations worldwide showed that the distribution of the different brGDGTs varies with annual mean air temperature (MAT) and soil pH; the number of cyclopentane moieties is related to soil pH, whereas the number of methyl branches is related to MAT and, to a lesser extent, also to soil pH (Weijers et al., 2007a). To quantify those changes, the Cyclisation of Branched Tetraethers (CBT) and Methylation of Branched Tetraethers (MBT) indices were developed, and defined as:

$$\mathrm{CBT} = -\mathrm{LOG}((\mathrm{Ib}+\mathrm{IIb})/(\mathrm{Ia}+\mathrm{IIa})) \quad (1)$$

$$\mathrm{MBT} = (\mathrm{Ia}+\mathrm{Ib}+\mathrm{Ic})/(\mathrm{Ia}+\mathrm{Ib}+\mathrm{Ic}+\mathrm{IIa}+\mathrm{IIb}+\mathrm{IIc}+\mathrm{IIIa}+\mathrm{IIIb}+\mathrm{IIIc}) \quad (2)$$

Roman numerals in the equations refer to the relative abundance of the molecules in Fig. 1. Based on the brGDGT distributions in a globally distributed soil calibration dataset, an equation to express CBT as function of soil pH was derived:

$$\mathrm{CBT} = 3.33 - 0.38 \times \mathrm{pH} \quad (n = 114;\ r^2 = 0.70) \quad (3)$$

Similarly, an equation for the relation of MBT with MAT and pH was derived:

$$\mathrm{MBT} = 0.867 - 0.096 \times \mathrm{pH} + 0.021 \times \mathrm{MAT} \quad (n = 114;\ r^2 = 0.82) \quad (4)$$

Correlation with CBT index instead of pH consequently results in a function to derive MAT based on the distribution of brGDGTs only:

$$\mathrm{MBT} = 0.122 + 0.187 \times \mathrm{CBT} + 0.020 \times \mathrm{MAT} \quad (n = 114;\ r^2 = 0.77) \quad (5)$$

The root mean square error (RMSE) for soil pH and MAT estimates is 0.7 and 4.8 °C, respectively. These relatively large errors indicate that the absolute values that are reconstructed with these proxies must be interpreted with caution.

While based and calibrated on soils, the MBT–CBT paleotemperature proxy (i.e. Eq. (5)) has so far mostly been applied on coastal marine sediment cores, where brGDGTs are likely deposited as part of river transported soil organic matter (Hopmans et al., 2004; Huguet et al., 2007; Walsh et al., 2008). Hence, down-core analysis of brGDGT distributions in river fan sediments results in an integrated climate record of the river basin. In this way, paleoclimate reconstructions have been made for e.g. tropical central Africa (Weijers et al., 2007b), the Lomonosov Ridge in the Arctic (Weijers et al., 2007c), Greenland (Schouten et al., 2008), the land surrounding the Skagerrak (Rueda et al., 2009), and the Amazon basin (Bendle et al., 2010). The MBT–CBT proxy has also been applied in the terrestrial realm itself. Analysis of brGDGTs in a Pliocene peat deposit in the Canadian Arctic provided insight in Arctic air temperatures during this time (Ballantyne et al., 2010), whereas brGDGTs in a loess-paleosol sequence from the Chinese loess plateau revealed the timing and magnitude of deglacial atmospheric warming in East Asia (Peterse et al., 2011). Application of this proxy to lake sediments, however, showed that the distribution of brGDGTs in the sediments of Lake Challa in equatorial West Africa, and Lake Towuti in Indonesia differs from that in the surrounding soils (Sinninghe Damsté et al., 2009; Tierney and Russell, 2009). Therefore, *in situ* production was suggested as a source of brGDGTs, in addition to those derived from erosion of soils in the lake catchment. The mixed provenance of brGDGTs in lakes complicates the application of the MBT–CBT proxy in these settings, and tends to result in a large underestimation of MAT (Blaga et al.,

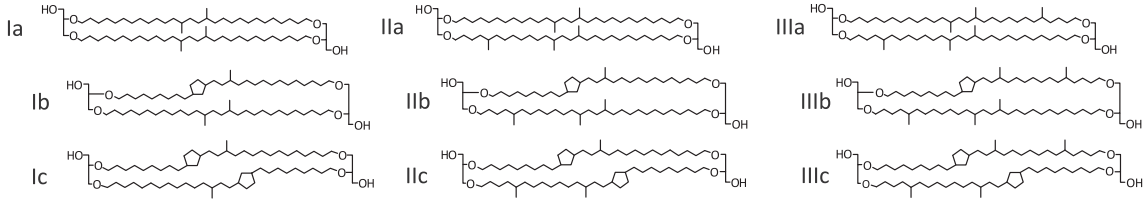

Fig. 1. Molecular structures of the branched GDGTs.

2010; Tierney et al., 2010a, 2012; Zink et al., 2010; Sun et al., 2011; Pearson et al., 2011). The MBT–CBT proxy has therefore been statistically assessed on local (e.g. tropical East Africa, Tierney et al., 2010a) as well as global scale (Sun et al., 2011; Pearson et al., 2011) to derive brGDGT-based temperature proxies that are applicable in lakes. This resulted in improved correlations for lacustrine brGDGTs and temperature, and suggests that a statistical approach may also be a promising method to improve the MBT–CBT proxy for application in soils, peats, or coastal marine sediments.

In soils, the uncertainty in the calibration may be a product of temperature differences between air used in the calibration, and soil, where the brGDGT producing bacteria live (Weijers et al., 2007a; Peterse et al., 2009c). Furthermore, differences in vegetation cover, or a seasonal bias may be introduced to the temperature signal on locations where brGDGT producing bacteria likely have a preferential growing season (e.g. Weijers et al., 2007c).

In this study we tried to improve the accuracy of the proxy by extending the original soil data set of Weijers et al. (2007a) by adding 126 new surface soils from globally distributed locations, and combining that with previously reported brGDGT distributions in 65 soils from China (Peterse et al., 2009b), the Amazon (Peru, Ecuador, Brazil, Colombia; Bendle et al., 2010), and Svalbard (Peterse et al., 2009a). Besides recalibrating the empirical MBT–CBT proxy based on the extended dataset, we also used a statistical approach to derive other combinations of brGDGTs that may improve their relation with temperature and soil pH. Finally, the new calibration function was tested by applying it on previously published MBT–CBT-derived MAT records.

2. MATERIALS AND METHODS

2.1. Soil dataset compilation

Of the initial global soil calibration set published by Weijers et al. (2007a), only the surface soils (0–10 cm) were selected for the new calibration set. This set was extended with newly analyzed surface soils from North-America, France, Chile, The Netherlands, Egypt and Uganda. Previously reported brGDGT distributions in soils from the Amazon (Peru, Ecuador, Brazil, Colombia; Bendle et al., 2010), Svalbard (Peterse et al., 2009a) and China (Peterse et al., 2009b) were added to complete the data set. The final soil collection is composed of 278 globally distributed surface soils (Fig. 2; Supplementary Table 1).

2.2. Branched GDGT analysis

The surface soils were freeze dried, powdered, and extracted (3×) with a mixture of dichloromethane (DCM):methanol (MeOH) 9:1 (v/v), using a DIONEX accelerated solvent extractor (ASE 200) at 100 °C and a pressure of 7.6×10^6 Pa for 5 min. The extracts were dried under near vacuum using a rotary evaporator, then dissolved in DCM and passed over a Na_2SO_4 column to remove any remaining water. Separation of the extracts in an apolar and a polar fraction was done by passing them over an activated Al_2O_3 column using hexane:DCM 9:1 (v/v) and DCM:MeOH 1:1 (v/v), respectively. The polar fraction, containing the brGDGTs, was dried under N_2, dissolved in hexane:isopropanol 99:1 (v/v), and filtered through a 0.45 μm PTFE filter. The polar fractions were concentrated to about 3 mg/ml prior to analysis by high performance liquid chromatography/atmospheric pressure chemical ionization-mass spectrometry (HPLC/APCI-MS) on an Agilent 1100 series LC/MSD SL according to Schouten et al. (2007). Separation of the branched GDGTs was achieved on an Alltech Prevail Cyano column (150 mm × 2.1 mm; 3 μm) as described by Schouten et al. (2007), with minor modifications. In short, the compounds were eluted isocratically with 90% A and 10% B for 5 min at a flow rate of 0.2 ml/min, and then with a linear gradient to 16% B for 34 min, where A = hexane and B = hexane:isopropanol 9:1 (v/v). The injection volume was 10 μl per sample. Selective ion monitoring of the $[M+H]^+$ of the different branched GDGTs was used to detect and quantify them.

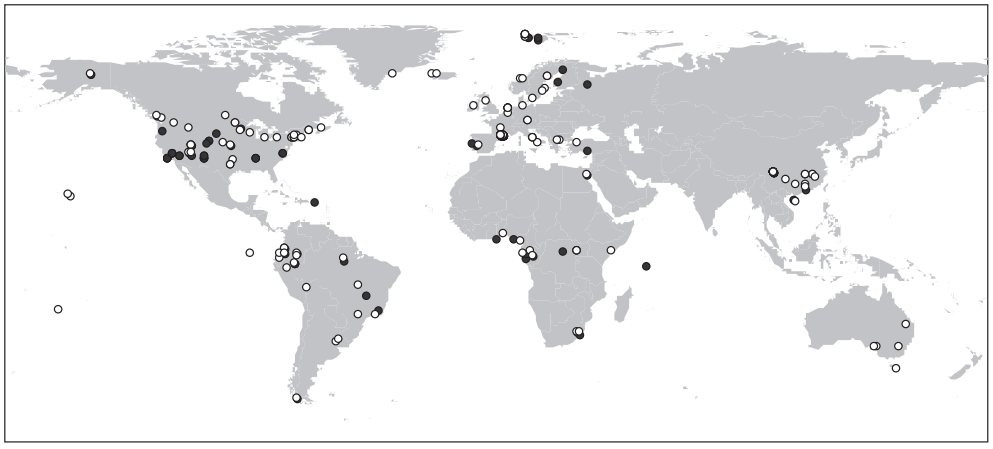

Fig. 2. Global overview map of the locations of surface soils used in this study. Open circles are soils included in the new calibration set ($n = 176$). The filled circles indicate soils that are excluded from the calibration set ($n = 102$) because one or more of the branched GDGTs are below detection limit.

2.3. Statistical analyses

Comparison of the relationships of brGDGT distributions with MAT and pH in subsets of, as well as in the complete dataset ($n = 278$) was done using a homogeneity of slopes test, followed by an analysis of covariance (ANCOVA) to compare slope and intercept, respectively. Significant differences between datasets are characterized by a Pearson's coefficient (p-value) < 0.05.

Principal component analysis (PCA) was performed on the relative abundances of the brGDGTs in the set of surface soils selected for the recalibration study, to provide a general view of the variability within the distribution of the brGDGTs. A second PCA biplot was generated for the environmental variables MAT, pH and MAP, as well as the MBT and CBT indices based on the same dataset.

A selection of 176 surface soils was used to derive new indices to describe the relations of brGDGT distributions with MAT and with soil pH with linear regression analysis, following the approach used for the TEX_{86} calibration by Kim et al. (2010a). In short, for each relation, the top hundred indices with the highest correlation coefficient were obtained according to the following format:

$$\text{Index} = \text{LOG}\left(\sum k_1 X / \sum k_2 X\right) \quad (6)$$

In this index, X refers to the relative abundance of one of the brGDGTs in a soil. The exact type of the brGDGT is represented by k_1 and k_2, the summation of which describes the numerator and the denominator, respectively. For each MAT and pH, the index with the highest correlation coefficient was selected for further testing. The obtained indices are expressed as a LOG-ratio to obtain a symmetrical distribution of the data points, which makes it easier to see the effect of increasing or decreasing index values (e.g. Montgomery and Peck, 1992).

Another set of equations to predict pH and MAT based on the distribution of brGDGTs was derived using least squares multiple linear regression analysis. This method assigns weighing factors to the fractional abundance of the individual branched GDGTs to obtain the equations with the highest coefficient of determination.

To assess the benefit of local calibrations of the MBT–CBT proxy, the spatial autocorrelation of brGDGT-based MAT and pH estimates in our set of surface soils was evaluated by performing a Moran's I test.

Redundancy analysis (RDA) was used to further assess the relationships of brGDGT distributions with the environmental parameters for which data was available. RDA is a form of constrained PCA, or a multivariate analogue of regression, and can be used to directly link components (in this case brGDGTs) with one or more explanatory variables (in this case MAT, pH and MAP). Subsequently, a series of partial RDAs were performed to constrain the unique and independent influence of each environmental parameter alone, as well as compared to all other parameters. The significance of the explanatory variances within a 1% confidence interval was tested with a permutation test.

All statistical analyses were performed with the R package, except for the multiple linear regression analysis, homogeneity of slopes test, and ANCOVA, which were performed using SYSTAT 12 and 13.

3. RESULTS AND DISCUSSION

3.1. BrGDGT distribution in surface soils

In this study we analyzed 126 surface soils and combined this with previously published data from 152 surface soils (see Section 2.1). In contrast to the original soil calibration dataset of Weijers et al. (2007a), where a number of deeper soil horizons was included in the dataset, we have restricted our dataset to surface soils only, as these likely experience the most direct influence of MAT. Furthermore, brGDGTs in coastal marine sediments, where the MBT–CBT proxy is frequently applied, are likely mainly derived from eroded surface soils on nearby land.

BrGDGTs were detected in all 278 surface soils, although not every soil contains the complete suite of brGDGTs, i.e. only 74 (26%) of the soils contain detectable amounts of all nine brGDGTs (Supplementary Table 1). In particular, brGDGTs-IIIb and IIIc (Fig. 1) are frequently below detection limit and, if present, do not comprise more than 1% of total brGDGTs on average. The most dominant brGDGTs are Ia, IIa and IIIa, while brGDGTs with cyclopentane moieties are generally present in lower amounts.

For the assessment of the relationship between environmental parameters and GDGT distributions it would be preferable to use only those soils that contain all nine brGDGTs. However, because this data set comprises only 74 soils, we excluded brGDGT-IIIb and IIIc from further analysis, since IIIb and IIIc are generally below the detection limit and, if detected, occur only in low abundance. The effect of excluding brGDGT-IIIb and IIIc on the relationships of MBT with MAT was tested on the original calibration dataset of Weijers et al. (2007a). Although the correlation coefficient for the MBT–MAT relation decreased from $r^2 = 0.67$ ($n = 134$, $p < 0.0001$) to $r^2 = 0.57$ ($n = 102$, $p < 0.0001$), the RMSE is only slightly smaller for the dataset based on 7 brGDGTs (5.2 °C vs. 5.1 °C), and the two relationships do not significantly differ in slope (homogeneity of slopes test: df = 1,232, $F = 0.174$, $p = 0.677$) or intercept (ANCOVA: df = 1,233, $F = 0.001$, $p = 0.971$), indicating no direct disadvantage of the removal of the two brGDGTs. The CBT index does not comprise brGDGT-IIIb and IIIc and is, therefore, not affected by their exclusion.

Projecting these results on the new dataset, this leaves 176 (or 63%) of the surface soils that contain quantifiable amounts of the seven remaining brGDGTs for the calibration (filled circles, Fig. 2). We tried to extend this dataset by excluding even more brGDGTs (e.g. IIc and Ic), but the balance between excluding as many minor brGDGTs as possible without losing too much information was found at the exclusion of only brGDGTs-IIIb and IIIc. This selection should not have major implications for general paleorecord applications of the proxy.

To examine the relationships of the relative abundances of the seven different brGDGT types with environmental parameters, we plotted their individual abundances (as a

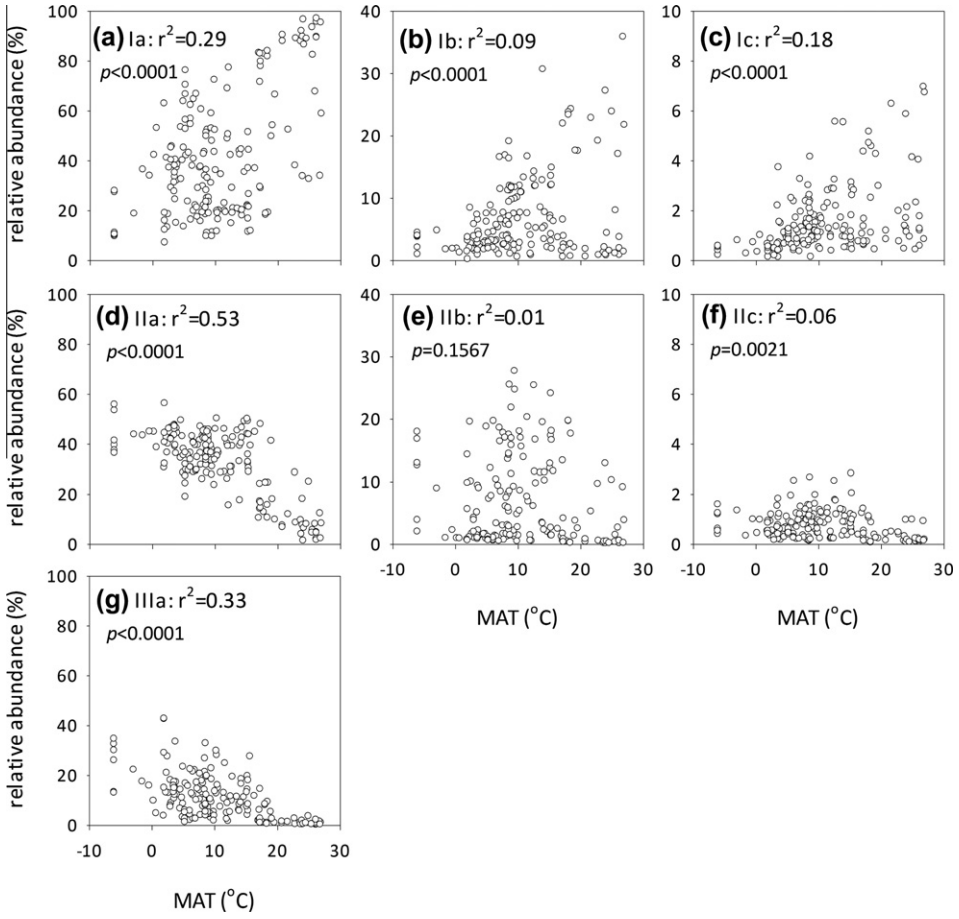

Fig. 3. Plots of the relative abundance of each individual branched GDGT (as a percentage of the sum of the seven selected branched GDGTs) versus MAT; (a) Ia, (b) Ib, (c) Ic, (d) IIa, (e) IIb, (f) IIc, (g) IIIa. Determination coefficients indicate those of a linear regression.

percentage of total brGDGTs) versus MAT and pH, respectively (Figs. 3 and 4). BrGDGTs without cyclopentane moieties show the strongest linear relationship with MAT. BrGDGT-IIa and IIIa negatively relate with MAT, while brGDGT-Ia shows a positive relation. This confirms that the number of methyl branches attached to the tetraether backbone of the brGDGTs decreases with increasing MAT (Weijers et al., 2007a; Peterse et al., 2009c). The other brGDGTs show mainly scatter or a weak relation with MAT (e.g. brGDGT-Ic, Fig. 3c).

The individual relations of the seven brGDGTs with pH are generally stronger than those with MAT (Fig. 4). Most of the brGDGTs with cyclopentane moieties show a positive exponential relation with pH, whereas brGDGT-Ia is the only GDGT that is negatively related with pH, and brGDGTs-Ic and IIa show no significant relation. As pH is a logarithmic function of the proton concentration in a soil, the exponential nature of the GDGT-pH relations supports the idea that soil pH influences the degree of cyclisation of brGDGTs (cf. Weijers et al., 2007a; Peterse et al., 2010). The relatively strong relation between brGDGT-Ia and pH indicates that also the degree of methylation is, to some extent, dependent on pH (cf. Weijers et al., 2007a).

Principal component analysis (PCA) on the relative abundances of the brGDGTs in these surface soils shows that the first two axes explain a cumulative of 82% of the variance in the data (Fig. 5). On the first principal component, explaining 49% of the variance, the score of GDGT-Ia is opposite to that of all other brGDGTs, especially GDGTs-IIb and IIc. BrGDGTs-Ic and Ib stand out on the positive side of the second factor (explaining 33% of the variance), against brGDGTs-IIa and IIIa, which have the highest negative scores on this factor.

3.2. Recalibration of the MBT–CBT proxy

Based on the relative abundance of the brGDGTs in the surface soils in the new dataset, we recalibrated the MBT and CBT indices. Before the calibration exercise, the MBT index was redefined as follows, since brGDGTs-IIIb and IIIc were excluded in the new surface soil dataset:

$$\mathrm{MBT}' = (\mathrm{Ia}+\mathrm{Ib}+\mathrm{Ic})/(\mathrm{Ia}+\mathrm{Ib}+\mathrm{Ic}+\mathrm{IIa}+\mathrm{IIb}+\mathrm{IIc}+\mathrm{IIIa}) \quad (7)$$

Correlation of the MBT′ and CBT indices with MAT and soil pH resulted in the following equations (Fig. 6a and b):

$$\mathrm{pH} = 7.90 - 1.97 \times \mathrm{CBT} \quad (n = 176;\ r^2 = 0.70;\ \mathrm{RMSE} = 0.8;\ p < 0.0001) \quad (8)$$

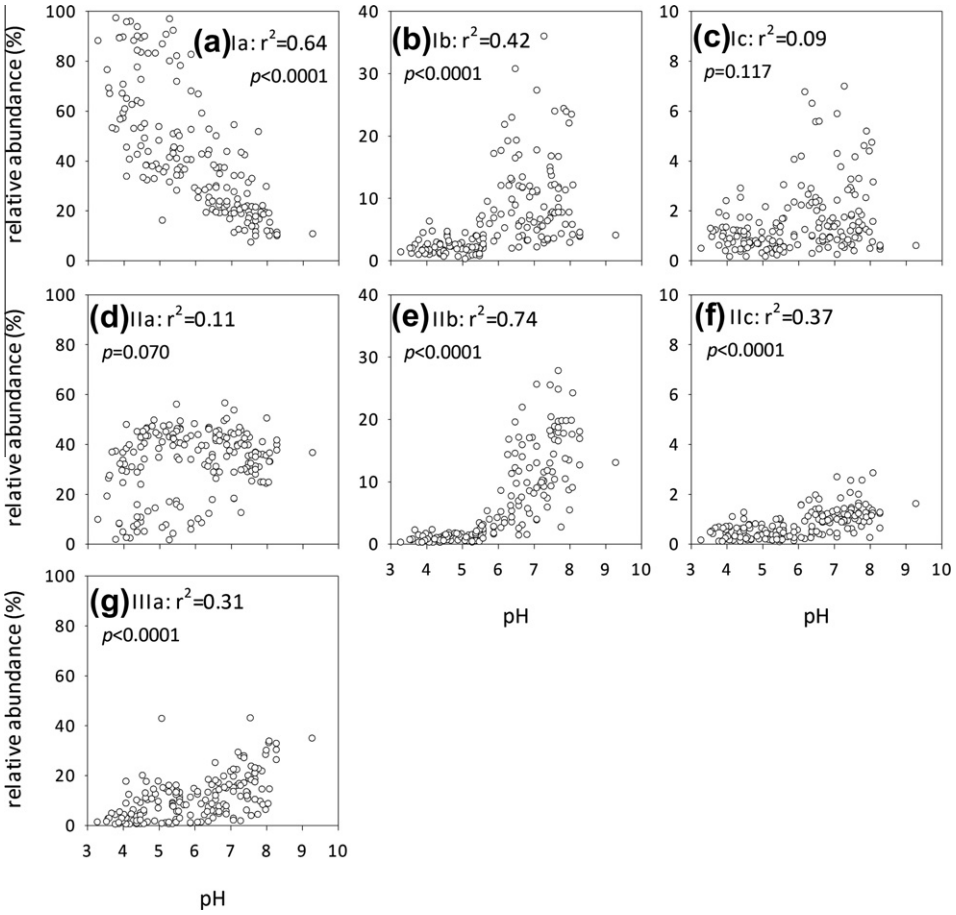

Fig. 4. Plots of the relative abundance of each individual branched GDGT (as a percentage of the sum of the seven selected branched GDGTs) versus soil pH; (a) Ia, (b) Ib, (c) Ic, (d) IIa, (e) IIb, (f) IIc, (g) IIIa. Determination coefficients indicate those of an exponential regression.

$$\mathrm{MAT} = -0.64 + 22.9 \times \mathrm{MBT}'$$
$$(n = 176;\ r^2 = 0.47;\ \mathrm{RMSE} = 5.7\ ^\circ\mathrm{C};\ p < 0.0001) \quad (9)$$

Similar to the original calibration set, no strong relation was observed between CBT and MAT, but MBT′ also relates significantly with soil pH:

$$\mathrm{pH} = 7.88 - 3.80 \times \mathrm{MBT}'$$
$$(n = 176;\ r^2 = 0.40;\ \mathrm{RMSE} = 1.1;\ p < 0.0001) \quad (10)$$

And MBT′ relates best with both soil pH and MAT:

$$\mathrm{MAT} = -23.20 + 2.86 \times \mathrm{pH} + 33.71 \times \mathrm{MBT}'$$
$$(n = 176;\ r^2 = 0.62;\ \mathrm{RMSE} = 4.8\ ^\circ\mathrm{C};\ p < 0.0001) \quad (11)$$

Thus, replacing pH by the CBT index and again performing linear regression analysis (cf. Weijers et al., 2007a), results in an equation that enables the estimation of MAT based on the CBT and MBT′ indices (Eqs. (1) and (7); Fig. 6c), i.e. the distribution of branched GDGTs:

$$\mathrm{MAT} = 0.81 - 5.67 \times \mathrm{CBT} + 31.0 \times \mathrm{MBT}'$$
$$(n = 176;\ r^2 = 0.59;\ \mathrm{RMSE} = 5.0\ ^\circ\mathrm{C};\ p < 0.0001) \quad (12)$$

The correlation coefficients of these new transfer functions are considerably lower than those of the original equations, i.e. Eqs. (3)–(5) (Weijers et al., 2007a), and the new MBT′–CBT calibration shows a relatively larger amount of scatter (Fig. 6c). Part of this scatter may be caused by the relatively large amount of soils from temperate regions that were added to the calibration set (Fig. 2, Supplementary Table 1). These samples show a large variation in MAT, pH and MAP, and generally plot right in mid-temperature region where the largest scatter in the original MBT–MAT plot of Weijers et al. (2007a) was already observed. We examined possible outliers by calculating standardized residuals for the MBT′–MAT and CBT–pH relationships. However, despite the increased scatter, the standardized residuals are generally between 2 and −2, indicating no outliers, and that the relationships are captured well by the empirically derived transfer functions (Fig. 6).

3.3. Statistical reevaluation of the relations between brGDGT distributions with MAT and soil pH

The original MBT and CBT indices were defined by empirically linking environmental controls with a presumed physiological mechanism of membrane adaptation by the soil bacteria producing the brGDGTs, i.e. an increase in the number of methyl branches with decreasing MATs,

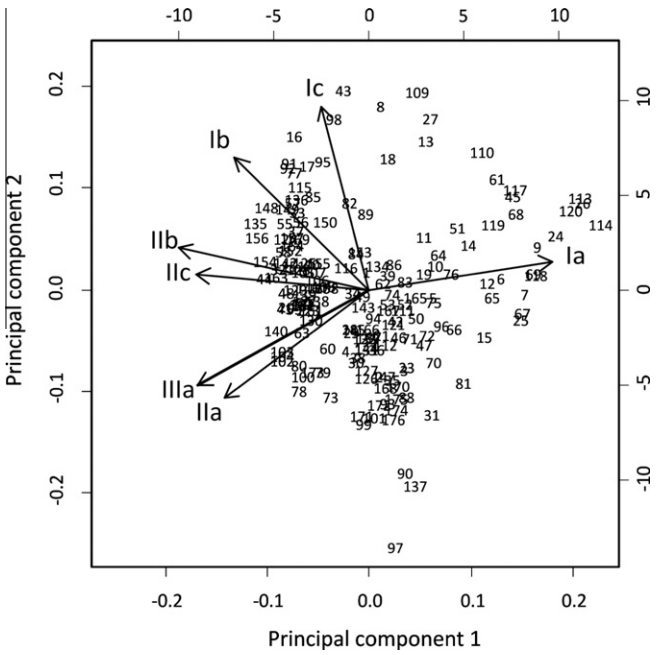

Fig. 5. Principal components analysis (PCA) biplot of the branched GDGT distributions in the surface soils of the extended global calibration set ($n = 176$). The first principal component explains 59.7%, and 26.2% of the variation is explained by the second principal component. Numbers in the biplot correspond to soils in Supplementary Table 1.

and the formation of additional cyclopentane moieties with increasing soil pH (Weijers et al., 2007a). An objective statistical approach for determining the best indices to describe the relations between brGDGTs, MAT and pH has so far been lacking. To examine this, we used linear regression analysis to compute the best combinations to describe MAT and pH based on the relative abundance of the previously selected seven brGDGTs in the extended global surface soil calibration set. The following index gave the best relation with MAT:

$$\text{Index} - 1 = \text{LOG}(\text{Ic}/\text{IIIa}) \quad (13)$$

$$\text{MAT} = 16.5 + 7.96 \times \text{Index} - 1 \quad (n = 176;\ r^2 = 0.60;\ \text{RMSE} = 4.9\ ^\circ\text{C};\ p < 0.0001) \quad (14)$$

For soil pH, the following index and equation were obtained:

$$\text{Index} - 2 = \text{LOG}\left((\text{Ic} + \text{IIb})/(\text{Ia} + \text{Ib} + \text{Ic} + \text{IIc})\right) \quad (15)$$

$$\text{pH} = 7.94 + 2.00 \times \text{Index} - 2 \quad (n = 176;\ r^2 = 0.78;\ \text{RMSE} = 0.7;\ p < 0.0001) \quad (16)$$

Strikingly, index-1 is much simplified over the MBT′ index, while index-2 uses more individual brGDGTs compared to the CBT index. Although the determination coefficients for these new indices are slightly higher compared to the MBT′ and CBT index, the accuracy of the MAT and pH estimates is only marginally improved. Furthermore, both indices heavily rely on the relative abundance of brGDGT-Ic, which often comprises less than 2% of the total amount of brGDGTs, with maxima of 6% in a few soils from the humid tropics (Fig. 3c; Supplementary Table 1). The strong dependence on brGDGT-Ic, which is a minor brGDGT, would seriously limit the applicability of the indices to areas where brGDGT-Ic is above detection limit as well as quantification limit. Finally, the mathematics of these new indices are not directly in line with the presumed mechanism of cell membrane adaptation, i.e. variation in the degree of methylation and cyclisation of the membrane to adjust its fluidity and permeability.

Another method that can potentially improve the empirical relation between brGDGT distribution and environmental parameters is least squares multiple linear regression analysis. A recent application of this method on brGDGT distributions in East African lakes showed that the accuracy of MAT estimates improved considerably relative to those derived with the original MBT–CBT proxy (Tierney et al., 2010a). The method assigns weighing factors to the fractional abundance of the individual brGDGTs to obtain the equation with the highest coefficient of determination for the estimation of MAT or pH. Application to our dataset resulted in the following equations:

$$\text{pH} = 8.49 - 0.043 \times \text{Ia} + 0.013 \times \text{Ib} + 0.019 \times \text{Ic} - 0.037 \times \text{IIa} + 0.045 \times \text{IIb} - 0.18 \times \text{IIc} + 0.020 \times \text{IIIa} \quad (n = 176;\ r^2 = 0.72;\ \text{RMSE} = 0.7) \quad (17)$$

$$\text{MAT} = 192.7 - 1.7 \times \text{Ia} - 1.6 \times \text{Ib} - 1.2 \times \text{Ic} - 2.0 \times \text{IIa} - 1.7 \times \text{IIb} - 3.3 \times \text{IIc} - 1.9 \times \text{IIIa} \quad (n = 176;\ r^2 = 0.60;\ \text{RMSE} = 4.9\ ^\circ\text{C}) \quad (18)$$

Again, the determination coefficients show only marginal improvements on the revised MBT′ and CBT relations. A similar observation is made when only the three

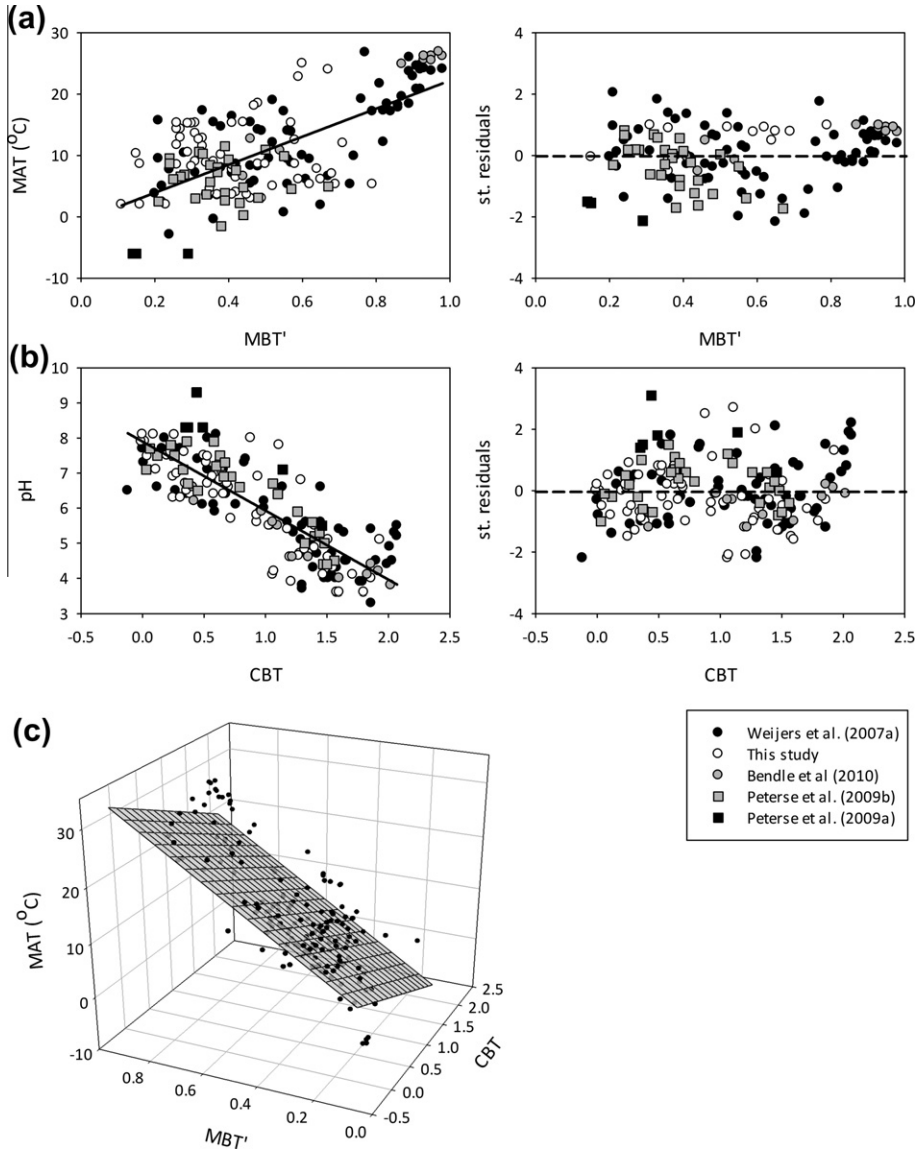

Fig. 6. Linear regression plots and standardized residuals for (a) MAT and MBT′, and (b) pH and CBT based on application of Eqs. (1) and (7), respectively, on the new global surface soil calibration set, and (c) 3D regression plot for the MBT′–CBT calibration on MAT (Eq. (12)). The different datasets of which the new calibration set is composed are distinguished by color or symbol.

major brGDGTs are used, i.e. Ia, IIa, and IIIa (cf. Tierney et al., 2010). This results in the following function:

$$\mathrm{MAT} = -70.4 + 89.2 \times \mathrm{Ia} + 70.0 \times \mathrm{IIa} + 84.9 \times \mathrm{IIIa} \quad (n = 248;\ r^2 = 0.16;\ \mathrm{RMSE} = 6.4\ ^\circ\mathrm{C}) \qquad (19)$$

The surprisingly poor relation of MAT using only the acyclic (i.e. type-a) brGDGTs shows that it is necessary to include cyclic compounds in the calibration in order to obtain a good fit with MAT, in contrast to those for lakes.

Thus, weighted calibrations, irrespective of the brGDGTs used, do not result in substantial improved relations. Therefore, we propose to use the MBT′ and CBT indices with their revised calibrations as proxies for paleotemperature and past soil pH.

3.4. Accuracy of MAT and pH estimates

The 3D calibration plot of the MBT′–CBT proxy has a considerable amount of scatter (Fig. 6c). The potential sources of this scatter, and possible solutions will be discussed below.

3.4.1. Soil temperature, vegetation, and seasonality

The scatter in the original calibration plot of Weijers et al. (2007a) was ascribed to the use of air temperature instead of *in situ* soil temperature, as well as to the heterogeneity of soils. Although 90% of the variation in soil temperature at 10 cm depth is generally explained by air temperature (Bartlett et al., 2006), the annual mean

temperature in a soil does not automatically resemble MAT at the same location, but also captures variations in e.g. incoming radiation (depending on vegetation type and seasonality), the heat capacity (depending on soil texture), or water content (depending on precipitation and evapotranspiration) of the soil (Smerdon et al., 2004). The importance of each of these additional factors, or combinations thereof, varies with latitude, although this does not lead to a systematic offset between air and soil temperature (Smerdon et al., 2004). Air and soil temperatures may be off by a few degrees when comparing them at a seasonal or annual interval, but this difference is reduced to only tenths of degrees on a centennial scale (Smerdon et al., 2006). Given the turnover time of the total brGDGT pool in a soil is with about 18 years (Weijers et al., 2010) relatively slow, it is likely that a decadal soil–air temperature offset in the order of about one degree may be responsible for some part of the scatter in the calibration. In a recent study, Weijers et al. (2011) indeed show that at 3 out of 4 locations for which both soil and air temperature data were available, brGDGT-reconstructed temperatures are closer to annual mean soil temperatures than to MAT, although the observed difference was mostly within the calibration error of the proxy. The same study also suggests a possible influence of vegetation cover on the distribution of brGDGTs. At two locations (in Ohio and Minnesota), the brGDGTs in three soils from the same site, but under different vegetation have a different distribution, and thus reconstructed MAT. When using air temperature for calibration purposes, these three soils would all be coupled to the same MAT, which would unavoidably introduce scatter to the calibration. Thus, it seems that the use of *in situ* soil temperature instead of MAT may help to reduce the scatter and improve the accuracy of the proxy. Unfortunately, the soil temperature data that would be needed to reduce this part of the scatter in the MBT′–CBT proxy calibration are currently not available for all individual locations on the appropriate time scale, i.e. annual mean temperatures over several decades, as they are for e.g. marine or lake temperatures. Thus, until this data becomes available we use the mean annual air temperature from nearby weather stations, which do have substantial spatial and temporal coverage.

Seasonality has also been put forward to explain part of the scatter (e.g. Weijers et al., 2007a; Rueda et al., 2009; Peterse et al., 2011). However, Weijers et al. (2007a) did not find better relations between seasonal temperatures and the MBT index than with MAT. Furthermore, no apparent seasonal pattern in the distribution of brGDGTs was found in mid-latitude soils (Weijers et al., 2011). Hence, the remaining scatter is unlikely to be fully explained by seasonality.

3.4.2. Local proxy calibrations

The use of a local rather than the global calibration has also been suggested as a possibility to improve the accuracy of brGDGT-derived temperature estimates (e.g. Sinninghe Damsté et al., 2008; Peterse et al., 2009c; Bendle et al., 2010). We, therefore, performed a Moran's I test on the new surface soil calibration set. A Moran's I test analyzes the degree of dependence in a geographical space, and thus indicates whether two soils that are located in close vicinity have a similar offset between estimated and measured MAT. Hence, application of local calibrations would become beneficial when soils from one geographical location all have the same temperature deviation. The spatial correlation in a dataset is indicated by a linearly increase in Moran's I. However, the test results for both MAT and pH show no indication of such trend (Fig. 7a and b, respectively), which implies that a local calibration will not likely lead to substantially improved accuracy. Plotting residual temperatures (i.e. the difference between measured and reconstructed MAT) for each soil in the calibration set on a global map further illustrates the absence of a systematic local offset, as there are no specific clusters with large residuals in certain regions (Fig 7c).

3.4.3. Influence of precipitation on brGDGT distributions

Next to MAT and soil pH, also soil moisture, or precipitation, seems to have an effect on brGDGT distributions (Weijers et al., 2007a). The relative abundance of some of the brGDGTs indeed relates with mean annual precipitation (MAP; Fig. 8), especially GDGTs Ia ($r^2 = 0.36$) and IIa ($r^2 = 0.41$). These brGDGTs contribute to the CBT as well as the MBT′ index, suggesting that variations in MAP may possibly affect the index values. However, like in the original calibration set of Weijers et al. (2007a), MAP and MAT are significantly correlated with each other ($r^2 = 0.31$; $p < 0.0001$), which makes it statistically nearly impossible to separate influences of MAT and MAP on brGDGT distributions. Indeed, MAT and MAP plot in the same quadrant in the PCA biplot showing the relations of environmental controls MAT, pH, and MAP as well as the MBT′ and CBT indices for the soils in the calibration set (Fig. 9a). The MBT′ index also plots in this quadrant, which confirms that the degree of methylation is mainly controlled by both MAP and MAT. Likewise, the opposite directions of the vectors representing soil pH and the CBT index represents the negative relation of soil pH and the degree of cyclisation of brGDGTs.

In another attempt to detangle the influence of temperature and precipitation on brGDGT distributions among the soils in the calibration set, we performed redundancy analysis (RDA) and variance partitioning on the relative abundances of the brGDGTs. The first three axes of the RDA together explain 53% of the variance. The first axis (Fig. 9b) explains 37.4% of the variance, and mainly reflects the variation in soil pH, with high pH soils plotting in the left part of the triplot, whereas soils with a lower pH plot more towards the right. The gradient of warm and wet soils in the lower part of the triplot, towards cold and dry soils in the upper part of the plot is captured by the second axis, and explains 15.2% of the variance. The partitioning analyses show that MAT, pH, and MAP all have a significant independent effect on the distribution of brGDGTs among the soils in our calibration set (Table 1). Soil pH is with 33.0% clearly the largest contributor to the explained variance. The explained variance remains relatively high when also taking the other environmental controls in account (i.e. 25.5%; Table 1), indicating that most of the explained variance can indeed be linked to changes in soil pH and

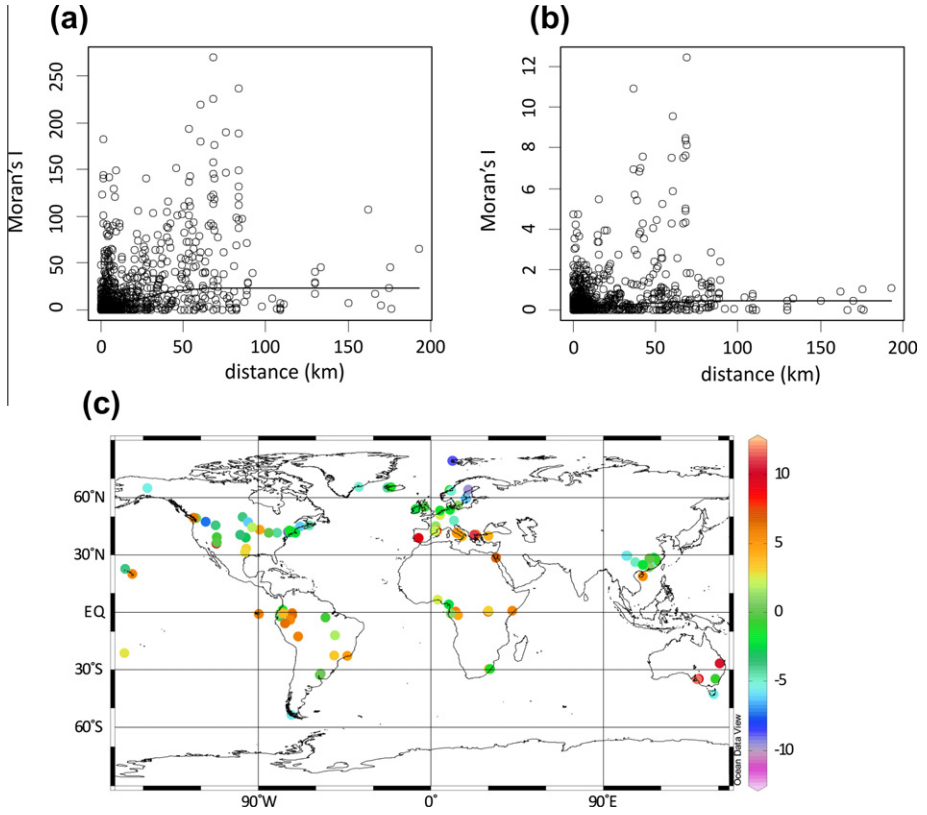

Fig. 7. Moran's I results for testing spatial autocorrelation of a) MAT and b) pH in the new surface soil calibration set ($n = 176$), and c) global overview map with residual temperatures (measured-MBT′–CBT-derived MATs).

is not related to co-varying changes in MAT or MAP. MAT and MAP, on the other hand, contribute to a smaller, but relatively equal amount of the explained variance. However, the unique contribution of MAT (9.4%) is higher than that of MAP (1.5%), which suggests that MAT has a slightly stronger control on the distribution of brGDGTs in this calibration set than MAP. The RDA results reflect the same ranking of the environmental parameters as controls on the relative abundance of the individual brGDGTs as was derived from Figs. 3, 4 and 8, i.e. pH > MAT > MAP. Nevertheless, the consequences of a possible significant impact of MAP on the distribution of brGDGTs, and thus on the MBT′ and CBT indices, may potentially be of most concern in areas where MAP and MAT are not positively related, i.e. in cold and wet, or in warm and dry areas.

This potential influence becomes visible when we plot MBT′–CBT-derived MATs using the revised soil calibration (Eq. (12)) versus measured MAT for the full (278) surface soil data set of this study (Fig. 10a), thereby assuming a 0% abundance for the brGDGTs which were below detection limit. The MAT scatter plot shows one cluster of soils for which the reconstructed MAT strongly underestimates actual MAT by up to 20 °C (Fig. 10a). The addition of precipitation data to this plot shows that this cluster mainly comprises alkaline soils from arid regions (MAP $\leqslant$ 500 mm; Fig. 10b) that are generally low in organic matter. This suggests that in these soil types, temperature is apparently no longer an important control on the distribution of brGDGTs. However, excluding all arid soils from the calibration dataset did not improve the relationship with MAT ($r^2 = 0.44$; $n = 154$). Although it is not possible to define an exact precipitation threshold or soil type for which the MBT′–CBT proxy should not be utilized, we suggest that MAT reconstructions for arid regions should be interpreted with care.

In summary, several factors may contribute to the scatter in the calibration between brGDGT distributions with MAT and pH. However, the relatively large uncertainty in absolute temperature estimates is likely to be mainly systematic. Hence, application of the proxy on a local scale, e.g. down core, results in temperature estimates with the same systematic error. As a consequence, the uncertainty on the trends in these paleotemperature records is likely to be much smaller compared to the uncertainties in absolute temperature estimates between different records (e.g., Tierney et al., 2010b; Peterse et al., 2011).

4. IMPLICATIONS FOR PALEOCLIMATE RECONSTRUCTION

To test the impact of the revised MBT′–CBT calibration on paleotemperature reconstructions, we derived new temperature records for the atmospheric warming in tropical Africa (Weijers et al., 2007b) and southeast Asia (Peterse et al., 2011) over the last deglaciation, the onset of long-term cooling near the Eocene–Oligocene (E–O) boundary

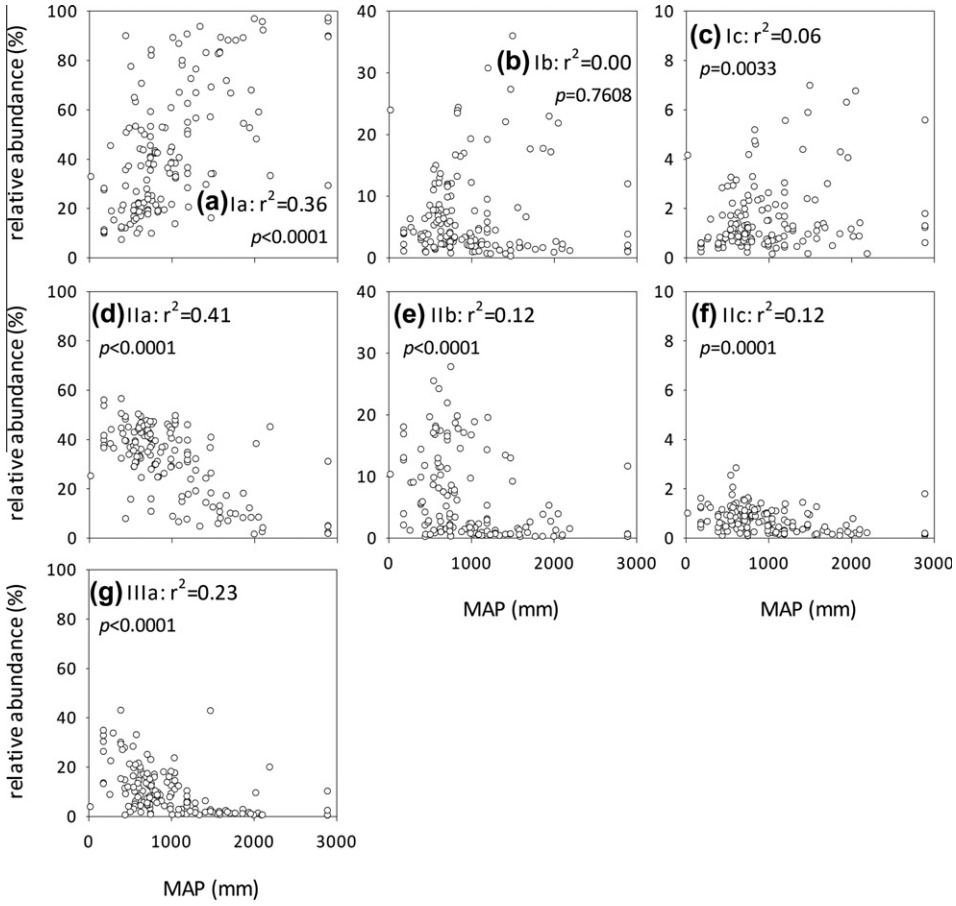

Fig. 8. Plots of the relative abundance of each individual branched GDGT (as a percentage of the sum of the seven selected branched GDGTs) versus MAP; (a) Ia, (b) Ib, (c) Ic, (d) IIa, (e) IIb, (f) IIc, (g) IIIa. Determination coefficients indicate those of a linear regression.

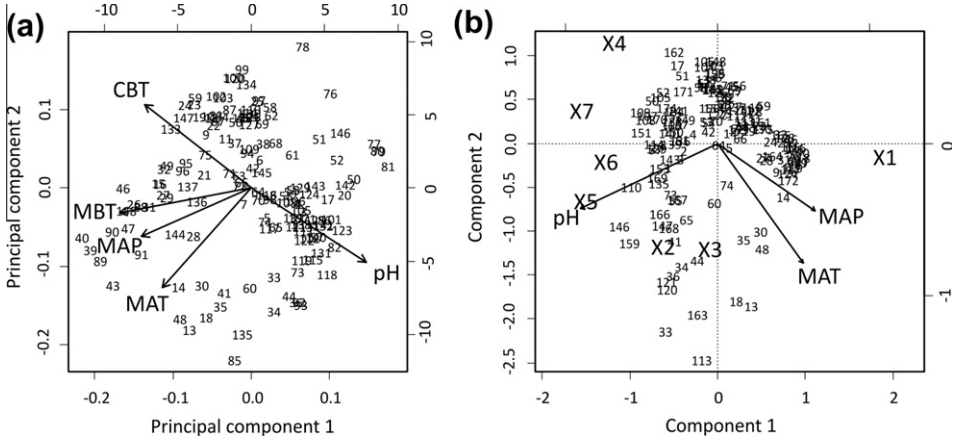

Fig. 9. (a) PCA biplot showing the relations between MAT, soil pH, MAP, the MBT′ and CBT indices, and the soils in the new soil calibration set ($n = 176$). The first component explains 60.4%, and the second component 24.7% of the variation. b) RDA triplot showing the relationships between the relative abundance of brGDGTs, soil pH, MAT, and MAP among the soils in the new soil calibration set ($n = 176$). Numbers in the plots correspond to soils in Supplementary Table 1.

(Schouten et al., 2008), and the period of extreme warmth during the PETM (Weijers et al., 2007c), and compared them with the records based on the original MBT–CBT calibration.

4.1. Deglacial atmospheric warming of tropical Africa

Application of the original MBT–CBT calibration in a sediment core recovered close to the Congo River outflow

Table 1
Results of RDA and partial RDAs indicating the total and individual contributions of soil pH, MAT, and MAP to the explained variance in brGDGT distribution among the soils in the calibration set. All components of variance are significant ($p < 0.01$).

Variable	Total (%)	Unique (%)
Soil pH	33.0	25.5
MAT	21.3	9.4
MAP	18.6	1.5
All variables	53.0	
Joint effects		16.6

suggested that MATs increased with ~0.7 °C/kyr from 20 to 21 °C during the Last Glacial Maximum (LGM) to a maximum of 25 °C in the first half of the Holocene (Fig. 11a, filled circles; Weijers et al., 2007b). The 24.5 °C that was reconstructed from the core-top sediment was similar to the present day MAT of the Congo River Basin (23.7 °C; Weijers et al., 2007b). Application of the newly calibrated MBT′–CBT shows the same temperature trends as the original MBT–CBT record (Fig. 11a, open circles), although absolute MAT estimates are lower, and now suggest MATs of 17.5 °C during the LGM, increasing to 20.5 °C during the Holocene. The brGDGT distribution in the surface sediment now suggests an air temperature of 20.5 °C, which is somewhat lower than the measured modern air temperature, although still well within the calibration error of the proxy. The LGM-Holocene temperature difference of ~3 °C is on the lower hand of the range indicated by other proxy records based on e.g. pollen assemblages (e.g. Bonnefille et al., 1990) and TEX_{86}-derived lake surface temperature (Powers et al., 2005), that Weijers et al. (2007b) compared their data with.

Weijers et al. (2007b) also used the CBT-derived pH record to reconstruct humidity changes in central Africa. The pH record based on the newly calibrated CBT index is almost identical to the original pH record, both in trend as in absolute values (Fig. 11b).

4.2. Deglacial atmospheric warming of East Asia

A continuous air temperature record for East Asia covering the last 34 kyr was derived from brGDGT distributions in a loess-paleosol sequence from the Mangshan loess plateau in China (Fig. 11c, filled circles; Peterse et al., 2011). The original record suggested a large increase in air temperature over the deglaciation with temperature estimates increasing from ~17 °C during the last glacial period to a maximum of ~27 °C during the Holocene climatic optimum. This temperature record is considered to be biased towards the summer, as the brGDGTs in the surface loess layer reflected average present day air temperatures of the monsoon and summer season (~24 °C). The air temperatures that are derived with the new MBT′–CBT calibration are lower than the original record, and now suggest air temperatures of ~15 °C for the LGM, increasing towards 21 °C in the Holocene (Fig. 11c, open circles). A deglacial warming of 6–7 °C, as indicated by the new record, falls in the temperature range based on the pollen and phytolith-derived reconstructions for this region as cited by Peterse et al. (2011). The temperature estimate of the surface layer, ~19 °C, suggests that the record is perhaps less biased towards summer temperatures, although it is still well above the present day MAT in this area of 13 °C. Irrespective of the lower absolute MAT estimates, which fall within the error of the proxies, the timing of the onset of deglacial atmospheric warming, and consequently the main conclusions of the original study, remain unaffected.

4.3. Oligocene–Eocene cooling of Greenland landmass

The climatic transition from a 'greenhouse' world to an 'icehouse' world took place around the E–O boundary (33.7 Ma BP), when the East Antarctic Ice Sheet first expanded. BrGDGTs from Greenland landmass, preserved in a marine sediment core from the Greenland Basin (ODP Site 913B), provided insight in the extent of atmospheric cooling in high-latitudes during this period (Schouten et al., 2008). Application of the original MBT–CBT

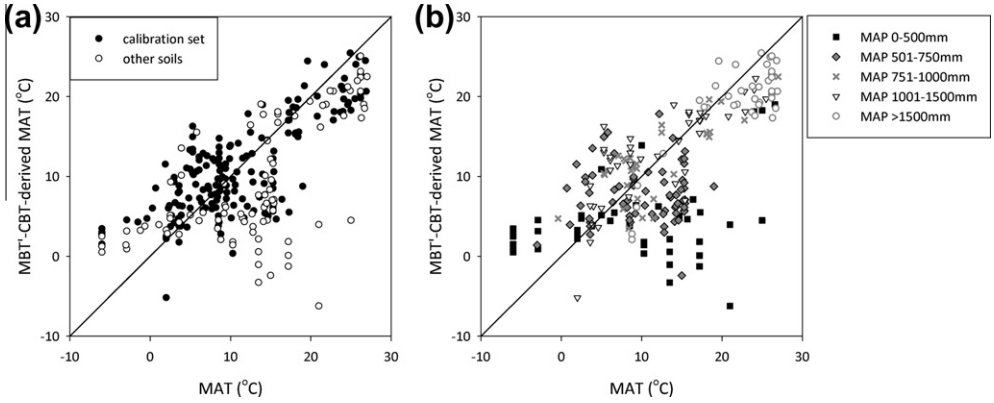

Fig. 10. MBT′–CBT-derived MAT estimates versus measured MAT for (a) the surface soils included in the MBT′–CBT global calibration set (filled circles; $n = 176$) as well as the soils that were excluded from the calibration set for which MAT was estimated by taking 0% for branched GDGTs below the detection limit (open circles; $n = 94$), and (b) soils for which MAP data were available ($n = 234$) divided in different precipitation classes. Line indicates 1:1 line where MBT′–CBT-derived MAT estimates equals measured MAT.

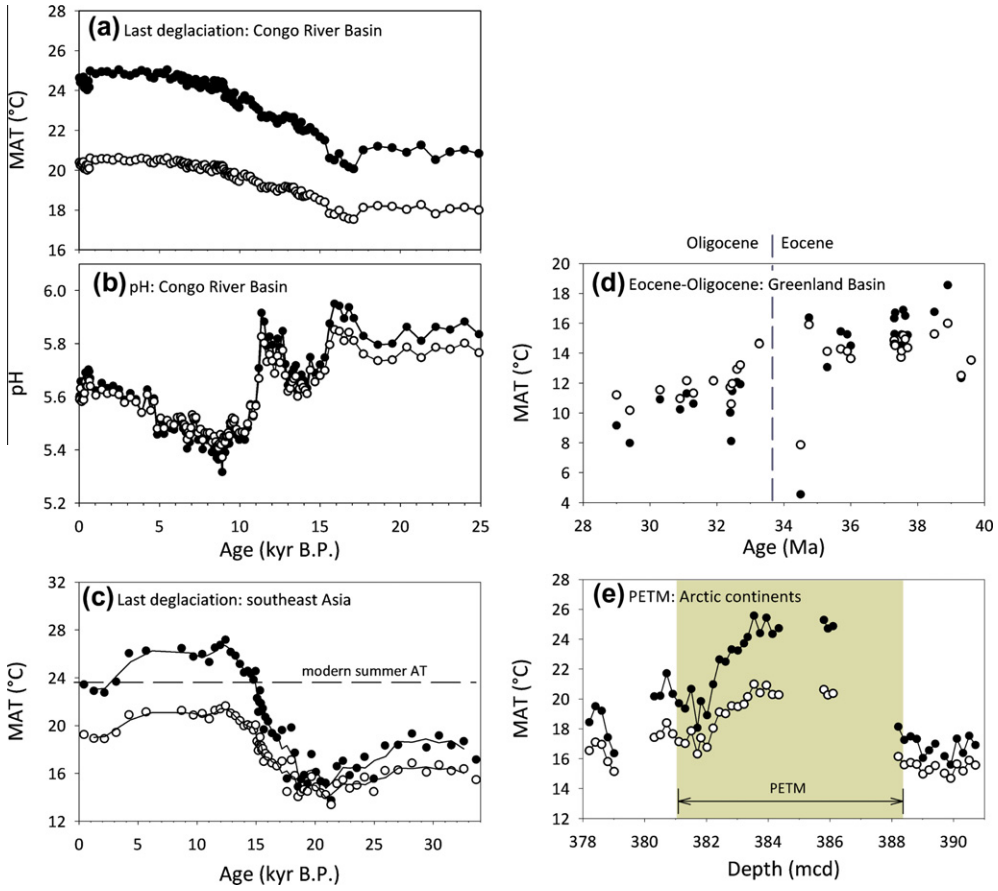

Fig. 11. Comparison of climate reconstructions based on the original MBT–CBT paleothermometer (Weijers et al., 2007a; filled circles) and based on the new MBT′–CBT calibration (open circles) for (a) the deglacial atmospheric warming and (b) pH record of tropical central Africa (Weijers et al., 2007b), (c) deglacial atmospheric warming in East Asia (Peterse et al., 2011), (d) the onset of long-term cooling of Greenland around the Eocene–Oligocene boundary (Schouten et al., 2008), and (e) the episode of extreme warmth during the PETM for the Arctic (Weijers et al., 2007c).

proxy suggested late Eocene air temperatures of 12–16 °C, dropping to 8–10 °C during the early Oligocene (Fig. 11d, filled circles), indicating a cooling of ~3–5 °C of the Greenland landmass. The absolute temperatures derived from the new MBT′–CBT calibration are similar to those reconstructed using the original indices, although the extent of the cooling is now smaller, i.e. ~2 °C (Fig. 11d, open circles). Application of Eq. (12) results in temperature estimates of 14 ± 1 °C for the Eocene, and 12 ± 1 °C for the early Oligocene, which fits independent temperature estimates based on pollen assemblages in the same, and nearby-located sediment cores, that indicate air temperatures of 14 ± 3 °C, decreasing to 10–11 $\pm$ 3 °C for the latest Eocene to Oligocene (Eldrett et al., 2009). Hence, the use of the new calibration does not affect the interpretation of high latitude climate development across the Eocene–Oligocene boundary.

4.4. Paleocene–Eocene thermal maximum at the Arctic

BrGDGTs originating from the Lomonosov Ridge, a land bridge in the central Arctic Ocean still elevated above sea level during the PETM, have been analyzed in a sediment core from the Arctic Ocean (IODP Hole 302-4A). The results indicate an atmospheric warming of ~8 °C during the PETM, above background values of ~17 °C (Fig. 11e, filled circles; Weijers et al., 2007c). These temperatures are considered to be relatively high, but were ascribed in part to a summer bias (Weijers et al., 2007c; Eberle et al., 2010). The new MAT estimates based on the MBT′–CBT proxy are 2 °C lower (~15 °C) for the late Paleocene and 3 °C lower (~21 °C) for the PETM compared to the original record (Fig. 11e, open circles). The previously observed trends in the temperature record remain unaffected but the magnitude of the warming decreases from 8 to 6 °C. The lower absolute MAT estimates and reduced amplitude of the record strongly resemble the temperature estimates based on leaf margin analyses by Wing et al. (2005), who reconstructed a MAT of ~15 °C for the late Paleocene, ~20 °C during the PETM, and ~18 °C for the early Eocene in Wyoming, United States. Furthermore, these lower temperatures are more consistent with MAT estimates based on e.g. pollen assemblages and oxygen isotopic compositions of fossil teeth and bones for the early Eocene Canadian Arctic (e.g. Eberle et al., 2010). This suggests that the use of the newly calibrated

MBT′–CBT proxy results in improved MAT estimates for this ancient greenhouse period.

5. CONCLUSIONS

Redefining the MBT index as MBT′ index by excluding rarely detected and quantifiable brGDGTs and extending the number of soils used for calibration of the MBT′–CBT proxy has led to new transfer functions to estimate MAT and soil pH. Attempts to improve the accuracy of the transfer functions with a statistical approach resulted in only marginally better correlation coefficients for the relations with MAT and pH, while their definition relate less well to the presumed physiological processes that are underlying the mechanism of the original MBT–CBT proxy. Thus, we propose to use the recalibrated MBT–CBT indices as originally defined by Weijers et al. (2007a), although in a slightly modified form (MBT′). Inspection of the large scatter in the MBT′–CBT calibration plot (Fig. 6c) indicated that brGDGT-based temperature estimates for arid soils may be underestimated by as much as 20 °C, and care should be taken with the interpretation of absolute temperature for arid regions.

Application of the new MBT′–CBT transfer function on previously published paleotemperature records from different locations and geological eras showed that the trends in the temperature reconstructions remain unchanged. The absolute temperature estimates, however, are generally lower, and often better match with temperature estimates for the same region and time interval based on independent proxies.

ACKNOWLEDGMENTS

We would like to thank three anonymous reviewers and Dr. T. Bianchi for their comments, which helped to improve this manuscript. Thanks also go to Jérôme Kaiser for soils from Chile, Cathelijne Stoof for the Portugese soil, and Lukas Jonkers for soil sampling in Egypt and Uganda. Barbara Zarzycka is thanked for help with collecting and processing the soils from the Têt river basin in France. This is publication number DW-2012-1005 of the Darwin Center for Biogeosciences, which partially funded this project by a grant to J.S.S.D. The research leading to these results has received funding from the European Research Council under the European Union's Seventh Framework Program (FP7/2007-2013)/ERC Grant agreement No. [226600]. F.P. acknowledges ETH Fellowship Grant FEL-36 11-1 for support.

APPENDIX A. SUPPLEMENTARY DATA

Supplementary data associated with this article can be found, in the online version, at http://dx.doi.org/10.1016/j.gca.2012.08.011.

REFERENCES

Ballantyne A. P., Greenwood D. R., Sinninghe Damsté J. S., Csank A. Z., Eberle J. J. and Rybczynski N. (2010) Significantly warmer Arctic surface temperatures during the Pliocene indicated by multiple independent proxies. *Geology* **38**, 603–606.

Bartlett M. G., Chapman D. S. and Harris R. N. (2006) A decade of ground–air temperature tracking at emigrant pass observatory. *Utah. J. Climate* **19**, 3722–3731.

Bendle J. A., Weijers J. W. H., Maslin M. A., Sinninghe Damsté J. S., Schouten S., Hopmans E. C., Boot C. S. and Pancost R. D. (2010) Major changes in glacial and Holocene terrestrial temperatures and sources of organic carbon recorded in the Amazon fan by tetraether lipids. *Geochem. Geophys. Geosys.* **11**, Q12007.

Blaga C. I., Reichart G.-J., Schouten S., Lotter A. F., Werne J. P., Kosten S., Mazzeo N., Lacerot G. and Sinninghe Damsté J. S. (2010) Branched glycerol dialkyl glycerol tetraethers in lake sediments: Can they be used as temperature and pH proxies?. *Org. Geochem.* **41** 1225–1234.

Bonnefille R., Roeland J. C. and Guiot J. (1990) Temperature and rainfall estimates for the past 40,000 years in equatorial Africa. *Nature* **346**, 347–349.

Colinvaux P. A., DeOliviera P. E., Moreno J. E., Miller M. C. and Bush M. B. (1996) A long pollen record from lowland Amazonia: Forest and cooling in glacial times. *Science* **274**, 85–88.

Eberle J. J., Fricke H. C., Humphrey J. D., Hackett L., Newbrey M. G. and Hutchison H. J. (2010) Seasonal variability in Arctic temperatures during the early Eocene time. *Earth Planet. Sci. Lett.* **296**, 481–486.

Eldrett J. S., Greenwood D. R., Harding I. C. and Huber M. (2009) Increased seasonality through the Eocene to Oligocene transition in northern high latitudes. *Nature* **459**, 969–974.

Hopmans E. C., Weijers J. W. H., Schefuß E., Herfort L., Sinninghe Damsté J. S. and Schouten S. (2004) A novel proxy for terrestrial organic matter in sediments based on branched and isoprenoid tetraether lipids. *Earth Planet. Sci. Lett.* **224**, 107–116.

Huguet C., Smittenberg R. H., Boer W., Sinninghe Damsté J. S. and Schouten S. (2007) Twentieth century proxies records of temperature and soil organic matter input in the Drammensfjord, southern Norway. *Org. Geochem.* **38**, 1838–1849.

Kim J.-H., van der Meer J., Schouten S., Helmke P., Willmott V., Sangiorgi F., Koc N., Hopmans E. C. and Sinninghe Damsté J. S. (2010a) New indices and calibrations derived from the distribution of crenarchaeal isoprenoid tetraether lipids: Implications for past sea surface temperature reconstructions. *Geochim. Cosmochim. Acta* **74**, 4639–4654.

Kurek J., Cwynar L. C., Ager T. A., Abbott M. B. and Edwards M. E. (2009) Late Quaternary paleoclimate of western Alaska inferred from fossil chironomids and its relation to vegetation histories. *Quat. Sci. Rev.* **28**, 799–811.

Lotter A. F., Birks H. J. B., Hofmann W. and Marchetto A. (1997) Modern diatom, cladocera, chironomid, and chrysophyte cyst assemblages as quantitative indicators for the reconstruction of past environmental conditions in the Alps. 1. *Climate J. Paleolimnol.* **18**, 395–420.

Montgomery D. C. and Peck E. A. (1992) *Introduction to Linear Regression Analysis*, 2nd ed. John Wiley & Sons, New York.

Pearson E. J., Juggins S., Talbot H. M., Weckström J., Rosén P., Ryves D. B., Roberts S. J. and Schmidt R. (2011) A lacustrine GDGT-temperature calibration from the Scandinavian Arctic to Antarctic: Renewed potential for the application of GDGT-paleothermometry in lakes. *Geochim. Cosmochim. Acta* **75**, 6225–6238.

Peterse F., Kim J.-H., Schouten S., Klitgaard Kristensen D., Koç N. and Sinninghe Damsté J. S. (2009a) Constraints on the application of the MBT/CBT palaeothermometer at high latitude environments (Svalbard, Norway). *Org. Geochem.* **40**, 692–699.

Peterse F., van der Meer M. T. J., Schouten S., Jia G., Ossebaar J., Blokker J. and Sinninghe Damsté J. S. (2009b) Assessment of soil *n*-alkane δD and branched tetraether membrane lipid distributions as tools for paleoelevation reconstruction. *Biogeosciences* **6**, 2799–2807.

Peterse F., Schouten S., van der Meer J., van der Meer M. T. J. and Sinninghe Damsté J. S. (2009c) Distribution of branched tetraether lipids in geothermally heated soils: Implications for the MBT/CBT temperature proxy. *Org. Geochem.* **40**, 201–205.

Peterse F., Nicol G. W., Schouten S. and Sinninghe Damsté J. S. (2010) Influence of soil pH on the abundance and distribution of core and intact polar lipid-derived branched GDGTs in soil. *Org. Geochem.* **41**, 1171–1175.

Peterse F., Prins M. A., Beets C. J., Troelstra S. R., Zheng H., Gu Z., Schouten S. and Sinninghe Damsté J. S. (2011) Decoupled warming and monsoon precipitation in East Asia over the last deglaciation. *Earth Planet. Sci. Lett.* **301**, 256–264.

Powers L. A., Johnson T. C., Werne J. P., Castañeda I. S., Hopmans E. C., Sinninghe Damsté J. S. and Schouten S. (2005) Large temperature variability in the southern African tropics since the Last Glacial Maximum. *Geophys. Res. Lett.* **32**, L08706.

Rueda G., Rosell-Melé A., Escala M., Gyllencreutz R. and Backman J. (2009) Comparison of instrumental and GDGT-based estimates of sea surface and air temperatures from the Skagerrak. *Org. Geochem.* **40**, 287–291.

Schouten S., Huguet C., Hopmans E. C., Kienhuis M. V. M. and Sinninghe Damsté J. S. (2007) Analytical methodology for TEX86 paleothermometry by high-performance liquid chromatography/atmospheric pressure chemical ionization-mass spectrometry. *Anal. Chem.* **79**, 2940–2944.

Schouten S., Eldrett J., Greenwood D. R., Harding I., Baas M. and Sinninghe Damsté J. S. (2008) Onset of long-term cooling of Greenland near the Eocene–Oligocene boundary as revealed by branched tetraether lipids. *Geology* **36**, 147–150.

Sinninghe Damsté J. S., Hopmans E. C., Pancost R. D., Schouten S. and Geenevasen J. A. J. (2000) Newly discovered non-isoprenoid glycerol dialkyl glycerol tetraether lipids in sediments. *Chem. Commun.* **17**, 1683–1684.

Sinninghe Damsté J. S., Ossebaar J., Schouten S. and Verschuren D. (2008) Altitudinal shifts in the branched tetraether lipid distribution in soil from Mt. Kilimanjaro (Tanzania): Implications for the MBT/CBT continental palaeothermometer. *Org. Geochem.* **39**, 1072–1076.

Sinninghe Damsté J. S., Ossebaar J., Abbas B., Schouten S. and Verschuren D. (2009) Fluxes and distribution of tetraether lipids in an equatorial African lake: Constraints on the application of the TEX86 palaeothermometer and BIT index in lacustrine settings. *Geochim. Cosmochim. Acta* **73**, 4232–4249.

Sinninghe Damsté J. S., Rijsptraa W. I. C., Hopmans E. C., Weijers J. W. H., Foesel B. U., Overmann J. and Dedysh S. N. (2011) 13,16-dimethyl octacosanedioic acid (*iso*-diabolic acid), a common membrane-spanning lipid of *Acidobacteria* subdivisions 1 and 3. *Appl. Env. Micr.* **77**, 4147–4154.

Smerdon J. E., Pollack H. N., Cermak V., Enz J. W., Kresl M., Safanda J. and Wehmiller J. F. (2004) Air-ground temperature coupling and subsurface propagation of annual temperature signals. *J. Geophys. Res.* **109**, D21107.

Smerdon J. E., Pollack H. N., Cermak V., Enz J. W., Kresl M., Safanda J. and Wehmiller J. F. (2006) Daily, seasonal, and annual relationships between air and subsurface temperatures. *J. Geophys. Res.* **111**, D07101.

Sun Q., Chu G., Liu M., Xie M., Li S., Ling Y., Wang X., Shi L., Jia G. and Lü H. (2011) Distributions and temperature dependence of branched glycerol dialkyl glycerol tetraethers in recent lacustrine sediments from China and Nepal. *J. Geophys. Res.* **116**, G01008.

Tierney J. E. and Russell J. M. (2009) Distributions of branched GDGTs in a tropical lake system: Implications for lacustrine application of the MBT/CBT paleoproxy. *Org. Geochem.* **40**, 1032–1036.

Tierney J. E., Russell J. M., Eggermont H., Hopmans E. C., Verschuren D. and Sinninghe Damsté J. S. (2010a) Environmental controls on branched tetraether lipid distributions in tropical East African lake sediments. *Geochim. Cosmochim. Acta* **74**, 4902–4918.

Tierney J. E., Mayes M. T., Meyer N., Johnson C., Swarenski P. W., Cohen A. S. and Russell J. M. (2010b) Late-twentieth-century warming in Lake Tanganyika unprecedented since AD 500. *Nat. Geosci.* **3**, 422–425.

Tierney J. E., Schouten S., Pitcher A., Hopmans E. C. and Sinninghe Damsté J. S. (2012) Core and intact polar glycerol dialkyl glycerol tetraethers (GDGTs) in Sand Pond, Warwick, Rhode Island (USA): Insights into the origin of lacustrine GDGTs. *Geochim. Cosmochim. Acta* **77**, 561–581.

Walsh E. M., Ingalls A. E. and Keil R. G. (2008) Sources and transport of terrestrial organic matter in Vancouver Island fjords and the Vancouver-Washington Margin: a multiproxy approach using $\delta^{13}C_{org}$, lignin phenols, and the ether lipid BIT index. *Limnol. Oceanogr.* **53**, 1054–1063.

Weijers J. W. H., Schouten S., Hopmans E. C., Geenevasen J. A. J., David O. R. P., Coleman J. M., Pancost R. D. and Sinninghe Damsté J. S. (2006) Membrane lipids of mesophilic anaerobic bacteria thriving in peats have typical archaeal traits. *Environ. Microbiol.* **8**, 648–657.

Weijers J. W. H., Schouten S., van den Donker J. C., Hopmans E. C. and Sinninghe Damsté J. S. (2007a) Environmental controls on bacterial tetraether membrane lipid distribution in soils. *Geochim. Cosmochim. Acta* **71**, 703–713.

Weijers J. W. H., Schefuß E., Schouten S. and Sinninghe Damsté J. S. (2007b) Coupled thermal and hydrological evolution of tropical Africa over the last deglaciation. *Science* **315**, 1701–1704.

Weijers J. W. H., Schouten S., Sluijs A., Brinkhuis H. and Sinninghe Damsté J. S. (2007c) Warm arctic continents during the Palaeocene–Eocene thermal maximum. *Earth Planet. Sci. Lett.* **261**, 230–238.

Weijers J. W. H., Wiesenberg G. L. B., Bol R., Hopmans E. C. and Pancost R. D. (2010) Carbon isotopic composition of branched tetraether membrane lipids in soils suggest a rapid turnover and a heterotrophic life style of their source organism(s). *Biogeosciences* **7**, 2959–2973.

Weijers J. W. H., Bernhardt B., Peterse F., Werne J. P., Dungait J. A. J., Schouten S. and Sinninghe Damsté J. S. (2011) Absence of seasonal patterns in MBT–CBT indices in mid-latitude soils. *Geochim. Cosmochim. Acta* **73**, 3179–3190.

Wing S. L., Harrington G. J., Smith F. A., Bloch J. I., Boyer D. M. and Freeman K. H. (2005) Transient floral change and rapid global warming at the Paleocene–Eocene boundary. *Science* **310**, 993–996.

Zink K.-G., Vandergoes M. J., Mangelsdorf K., Dieffenbacher-Krall A. C. and Schwark L. (2010) Application of bacterial glycerol dialkyl glycerol tetraethers (GDGTs) to develop modern and past temperature estimates from New Zealand lakes. *Org. Geochem.* **41**, 1060–1066.

Associate editor: Thomas S. Bianchi